ADDITIVELY MANUFACTURED CONFORMAL NEGATIVE STIFFNESS HONEYCOMBS

D. A. Debeau*, C. C. Seepersad*

*Department of Mechanical Engineering, The University of Texas at Austin, Austin, TX 78712

Abstract

This study investigates the static and dynamic mechanical performance of conformal negative stiffness honeycomb structures. Negative stiffness honeycombs are capable of elastically absorbing a static or dynamic mechanical load at a predefined force threshold and returning to their initial configuration after the load is released. Most negative stiffness honeycombs rely on mechanical loading that is orthogonal to the base of the structure. In this study, a more three dimensional design is presented that allows the honeycomb to conform to complex surfaces and protect against impacts from multiple directions. The conformal designs are additively manufactured in nylon and stainless steel and subjected to quasi-static mechanical loading and dynamic mechanical impact tests that demonstrate their impact protection capabilities.

Introduction

A honeycomb design that absorbs energy and mitigates mechanical impacts elastically is very desirable because it can recover from an initial impact and respond to a series of subsequent impacts. Conventional honeycombs and lattice structures provide lightweight strength and stiffness, but they absorb mechanical impacts plastically and therefore require replacement after each impact event. One way to achieve elastic collapse and recovery is to fabricate lattice structures with extremely thin, hollow walls [1], [2]. Another strategy is to incorporate curved or buckled beams that exhibit negative stiffness or snap-through behavior upon application of a mechanical load. These negative stiffness honeycombs appear in several instantiations in the literature [3] - [6], including an early design presented by the authors and illustrated in Figure 1 [7], [8].

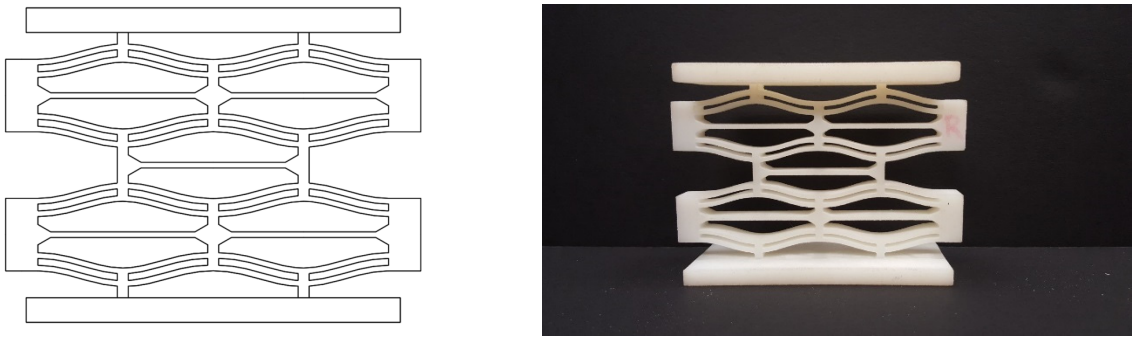

Figure 1. Negative Stiffness Honeycomb [7]

While the extruded two-dimensional honeycomb design in Figure 1 demonstrates nearly-ideal energy absorption (defined as mechanical energy absorption at constant force) under quasi-

static and dynamic mechanical loads [7], [9], it is difficult to utilize it in a three-dimensional environment. It does not conform well to nonplanar, three-dimensional underlying surfaces such as cylinders, spheres, or other curvaceous objects. Also, it performs best when the loading is orthogonal to its base, placing the honeycomb in compression. Any shear loading on the honeycomb could cause the structure to bend out-of-plane and eventually yield and break. To address these challenges, a conformal negative stiffness honeycomb design was developed, fabricated, and experimentally tested.

Conformal Negative Stiffness Element

The conformal negative stiffness element is illustrated in Figure 2. The geometry of the conformal element in Figure 2a is constructed by generating the profile for a unit cell from the previous design (Figure 2b) and revolving it 360° about its central axis, as shown in the cross-sectional view in Figure 2c. Then, four corners of the element are removed, as shown in the cross-sectional view in Figure 2d to form the conformal element in Figure 2a. The corners are removed for two reasons: (1) to facilitate powder removal when fabricating the elements with polymer or metal powder bed fusion (PBF), and (2) to allow the elements to be tiled conformally across a surface, as illustrated in Figure 3. As shown, tiling allows the elements to protect complex curved surfaces from impacts.

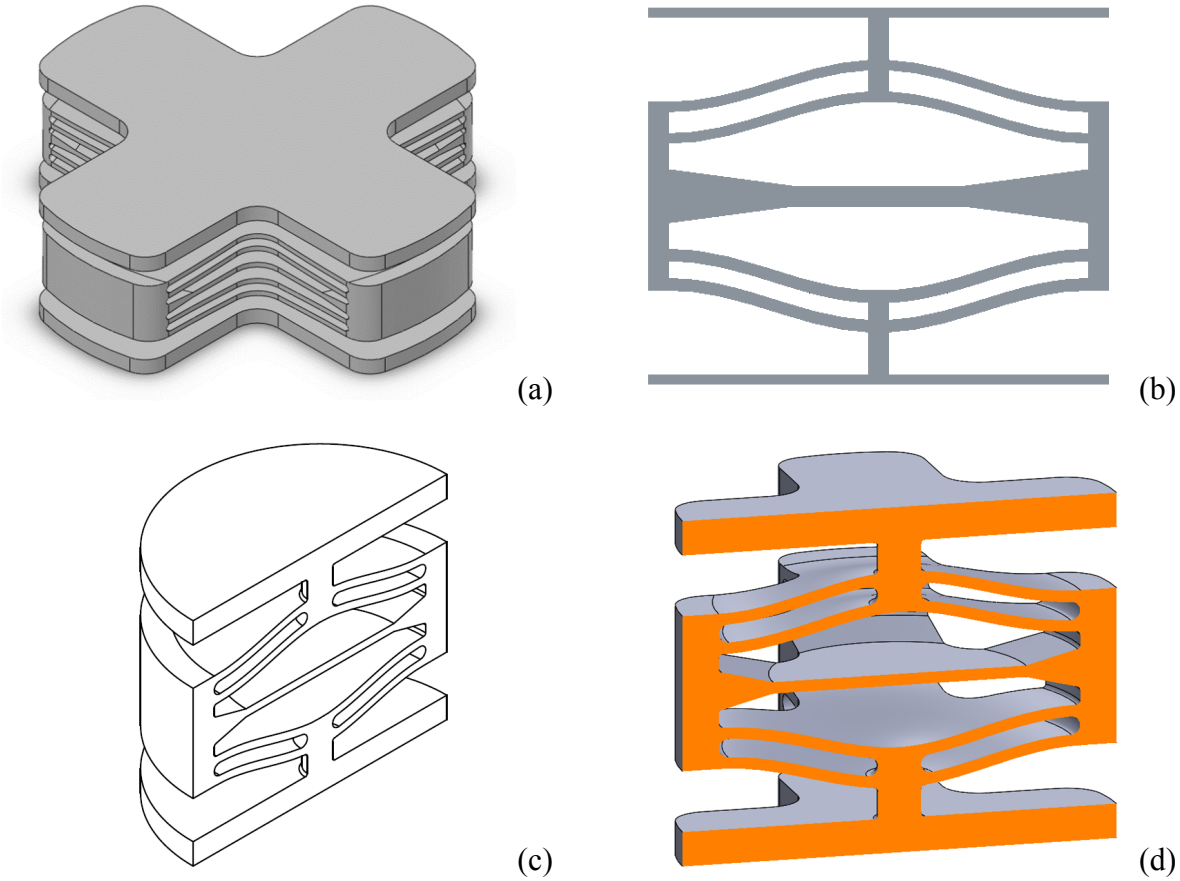

Figure 2. Conformal negative stiffness element (a) formed by revolving a unit cell cross section (b) about it central axis (c) and then removing four corners (d).

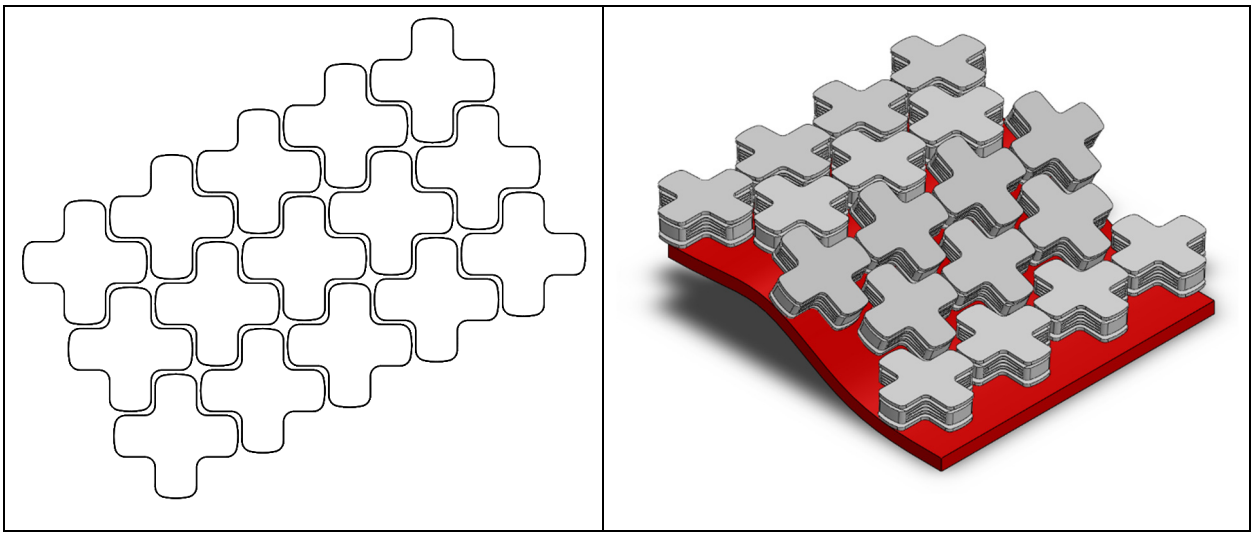

Figure 3. Conformal Elements Arranged in a Tiled Pattern

Conformal elements are designed to be fabricated with polymer and metal PBF in nylon 11 and 17-4PH stainless steel, respectively. Dimensions for the nylon 11 specimen are recorded in Figure 4. The curved shape of the beams is governed by the first mode shape of a buckled beam [10]. The dimensions of the beams are selected to achieve a prescribed force threshold, to prevent yielding of the beams, and to enable or prevent bistability, depending on the application.

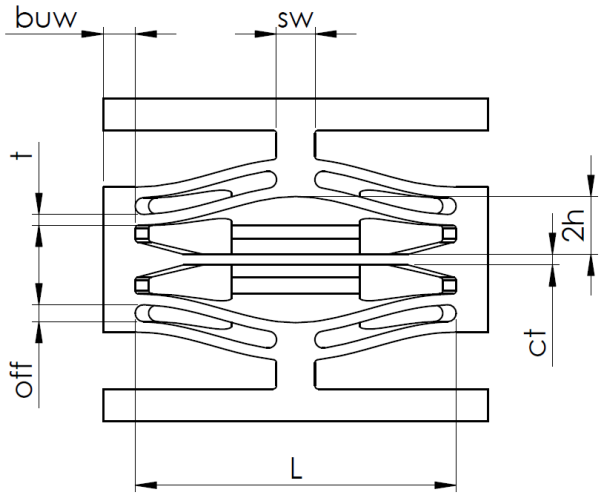

Critical Dimension	Value (mm)
Beam Thickness (t)	1.66
Center Thickness (ct)	1.66
Beam Length (L)	50.0
Bistability (Q)	2.71
Beam Height (h)	4.50 = Q * t
Beam Offset (off)	2.08 = 1.25 * t
Bumper Width (buw)	5.00
Stem Width (sw)	6.00

Figure 4. Section view and Dimensions of Nylon Design

Table 1. Selective Laser Sintered Nylon 11 Material Specifications, Obtained from a Tensile Bar Located Near the Specimens During the Build.

Material Specifications	**Value**
Young's Modulus (E)	1.21 GPa
Yield Strength (y)	30 MPa (approximate)
Yield Strain (emax)	0.10 (approximate)

The behavior of the beams is controlled by varying the thickness (t), length (L), and height (h), of the beams, as indicated in Figure 4. Increasing the thickness or height of the beam results in a higher force threshold, meaning more force required to snap the beam from one buckled shape to another, as described in [7], [8]. Increasing the length of the beam results in a lower force threshold, and reduces the maximum strain in the beam. According to Qiu *et al.* [10], the transverse displacement of the center of a curved beam is related to the transverse force applied to the center of the beam as follows:

$$F = \frac{3\pi^4 Q^2}{2}\Delta\left(\Delta - \frac{3}{2} + \sqrt{\frac{1}{4} - \frac{4}{3Q^2}}\right)\left(\Delta - \frac{3}{2} - \sqrt{\frac{1}{4} - \frac{4}{3Q^2}}\right) \quad (1)$$

Where F and Δ represent normalized force and normalized displacement, respectively. Those terms are related to applied transverse force, f, and transverse displacement, d, as follows:

$$F = \frac{fl^3}{E_s I h} \quad (2)$$

$$\Delta = \frac{d}{h} \quad (3)$$

In those expressions E_s is the modulus of elasticity of the cell wall material and I is the area moment of inertia of the cell wall. The maximum strain is governed by equation 4 [10].

$$\varepsilon_{max} \approx 2\pi^2 \frac{th}{L^2} + 4\pi^2 \frac{t^2}{3L^2} \quad (4)$$

Precise beam thickness and length values (as recorded in Figure 4) are chosen to avoid the yield strain/strength of the material (summarized in Table 1) and to be similar to those of previously fabricated specimens [7], which demonstrated highly repeatable performance.

Without exceeding the yield strength of the material, the beam height is varied to adjust the bistability parameter, or Q value, which is the ratio of beam height to thickness:

$$Q = h/t \quad (5)$$

The Q value can be used as a rough estimate of the transition between monostable and bistable buckling behavior [10]. Theoretically, beams with Q values below 2.31 are monostable and

return to their original state after the load is released. With Q values above 2.31, the beam is stable in two configurations (i.e., bistable) and requires an external force to return it to its original configuration. Bistability is not desirable in this application, because the structure would require external intervention to protect against multiple impacts. However, the equations underlying the transition value for Q assume that the boundaries of the curved beam are perfectly rigid. Since the beams are held in place by a framework with some elasticity, higher Q values are possible without bistability. In previous applications, Q values as high as 2.71 were embodied in nylon 11 (polymer PBF) versions of the honeycombs in Figure 1 without observing bistability. For the conformal specimens, the Q value is varied from 2.00 to 2.71 by adjusting the beam height.

The bumper width is set to a thickness that will not bend significantly under lateral loading from the curved beams as they snap through from one configuration to another. A thickness of 5 mm has been shown to adequately prevent this from happening in finite element simulations. The stem width is set to a thickness that will not shear under quasi-static loading. It can be increased if off-axis impacts are expected.

With the critical dimensions set, the force required to buckle the beams, or force threshold, can be estimated using equations 1, 2, and 3 [10]. Those equations are valid for standard curved beams, as illustrated in the original honeycomb design in Figure 1. To obtain the force threshold for a unit cell, the force threshold for a single curved beam is multiplied by two to account for double (concentric) beams in each instantiation. (The concentric beams encourage the beams to transition from a first-mode buckled shape to the opposite first-mode buckled shape via a third-mode, rather than a second-mode, buckled shape, thereby increasing the force threshold of the curved beams.) The same equations can be used to provide an estimate of the conformal design's force threshold, if it is assumed that the conformal design is equivalent to two intersecting unit cells of the original honeycomb design, as represented by the two intersecting rectangles in a top view in Figure 5.

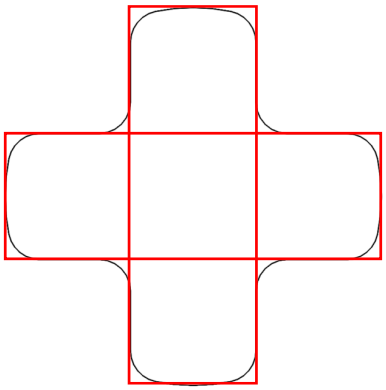

Figure 5. The Nylon Conformal Design Can Be Approximated as Two Intersecting Unit cells, as Shown in a Top View.

Dimensions for the 17-4PH stainless steel specimen are recorded in Figure 6. The material properties for 17-4PH Stainless Steel, fabricated with direct metal laser sintering (DMLS) are recorded in Table 2, as provided by the manufacturer for the production process described in the next section. Of the available DMLS materials, 17-4PH stainless steel was

selected for its low cost and high yield strain. The yield strain of the material was calculated using equation 6, based on the values in Table 2, with a safety factor (*sf*) to protect the beams from significant plastic deformation.

$$e_{max} = \log(1 + \frac{sf*y}{E} + 0.002) \quad (6)$$

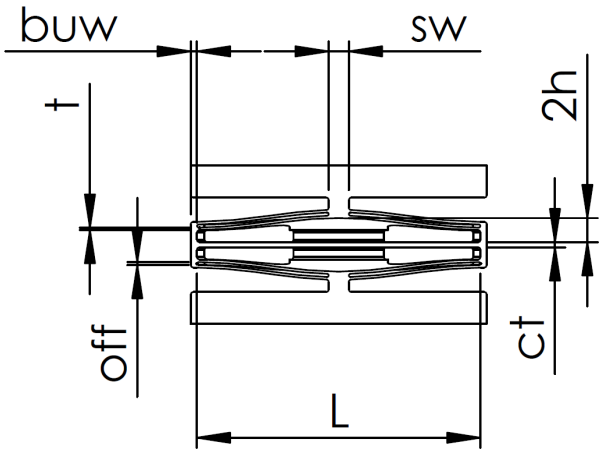

Critical Dimension	Value (mm)
Beam Thickness (t)	0.50
Center Thickness (ct)	1.00
Beam Length (L)	56.3
Beam Height (h)	2.41
Bistability (Q)	4.81
Beam Offset (off)	0.625
Bumper Width (buw)	5.00
Stem Width (sw)	4.00

Figure 6. Section View of Metal Design

Table 2 Additive Stainless Steel 17-4PH Material Specifications

Material Specifications	Value
Young's Modulus (E)	170 GPa
Yield Strength (y)	1241 MPa
Safety Factor (sf)	1.11
Yield Strain (emax)	0.0085

From past DMLS projects, it was known that features as thin as 0.5 mm could be reliably sintered. This dimension was selected as the beam thickness to maximize the height of the beam (and therefore the force threshold) without exceeding the allowable yield strain (according to Equations 4 and 6). With the beam thickness selected, the length of the beam was set to 55.5 mm to maximize the length of the beams without interfering with holes for mounting the specimen to testing equipment, as shown in Figure 7.

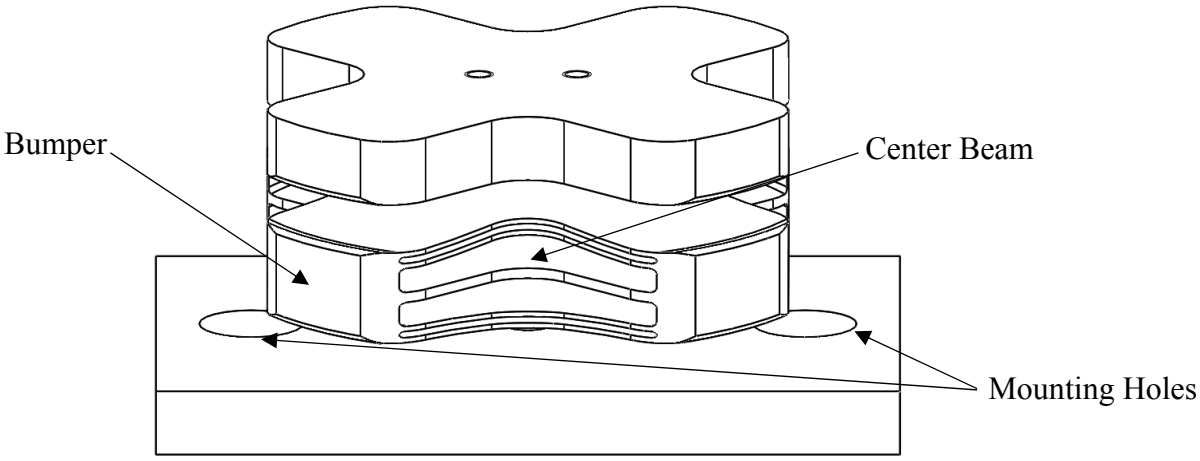

Figure 7. Metal Conformal Negative Stiffness Element

The center thickness was increased relative to the nylon designs to provide a stiffer brace for the four bumpers. FEA indicated that a center thickness equivalent to twice the thickness of the beams was large enough to prevent excessive lateral expansion of the bumpers. The offset thickness, bumper width, and stem width were set with criteria similar to the nylon design.

Manufacturing Methods

The nylon parts were selective laser sintered in PA D80-ST Nylon 11 from Advanced Laser Materials on a 3D Systems Sinterstation HiQ-HS . The layer thickness was set at 0.004 in, the laser power at 40.0 W, and the part bed temperature at 182.5 °C.

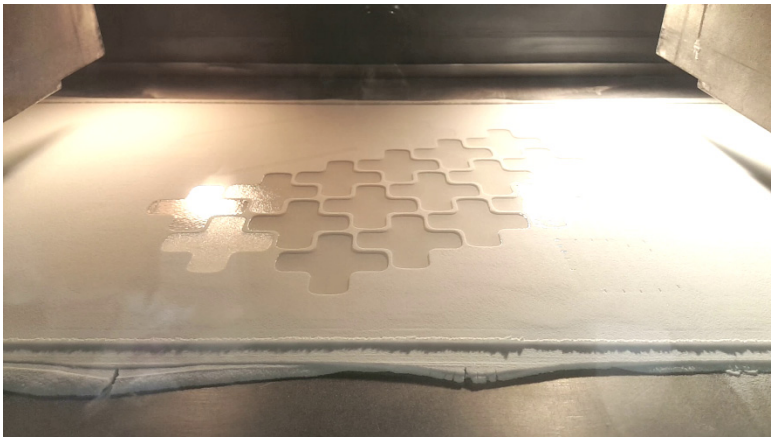

Figure 8. Selective Laser Sintering Process

The metal parts were manufactured on an EOS M270, with a layer thickness of 40 microns, using the standard EOS 17-4PH build settings. Four metal specimens in total were manufactured. A sintered specimen is shown in Figure 9. The specimens were built on their sides, as shown in Figure 10, in order to minimize the amount of support material needed. Nominally the overhang angle is 45 degrees, which is producible without support material in DMLS.

After the sintering process, the entire build plate was heated to a temperature of 1900 °F for an hour and then air cooled. This process reduces residual stresses in the part and helps prevent warping as parts are removed from the build plate. After the specimens were removed from the build plate, holes for mounting an accelerometer, and mounting the specimen to the drop table, were machined.

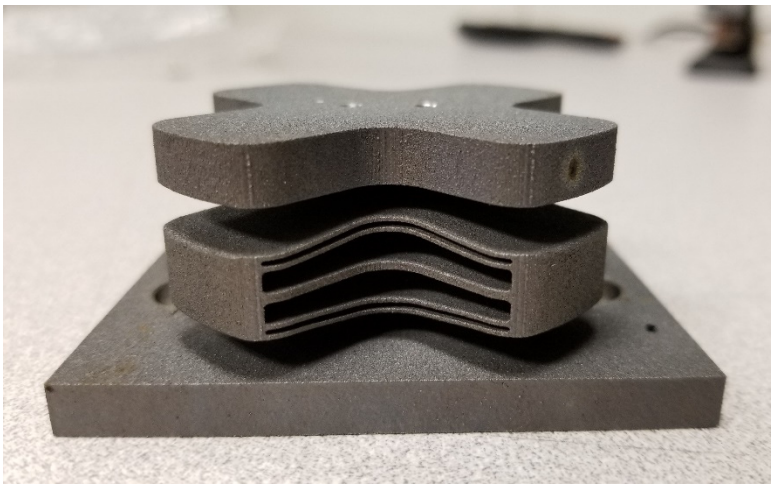

Figure 9. Sintered Specimen

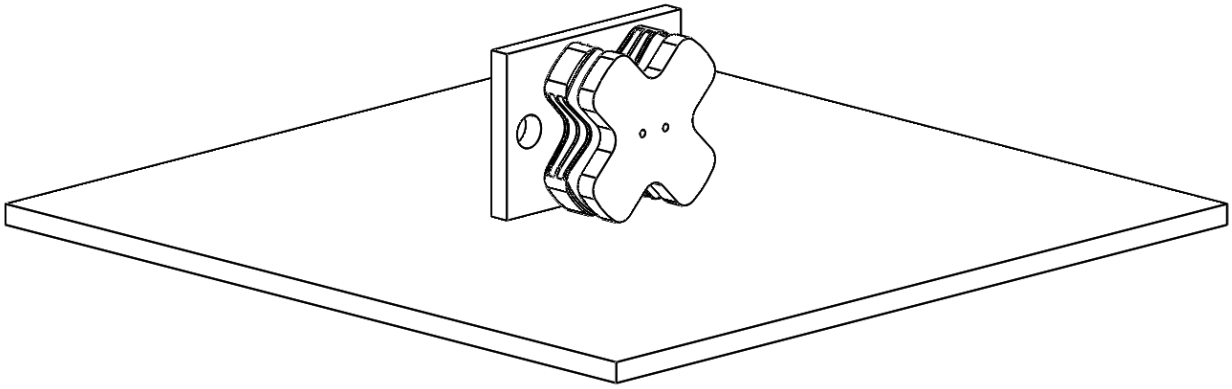

Figure 10. Build Orientation

After the machining process, the specimens were subjected to Hot Isostatic Pressing (HIP) to minimize residual porosity in the part. The HIP process subjects the part to 2125 °F, at 14.75 kpsi, for a nominal time of 4 hours. After the HIP process, the specimens were then hardened using the standard H1150 heat treat process, which requires heating to 1150 °F, for 4 hours and then air cooling. During the HIP and heat treat processes, the parts were oriented as shown in Figure 11. This allowed the parts to sag under their own weight, disrupting the intended geometry of the beams. Figure 11 shows specimen #1, which suffered the most damage from the processes. One specimen was heat treated separately, oriented on its side as in Figure 10, and did not suffer from sag; its performance is compared to the damaged specimens in the experimental results section.

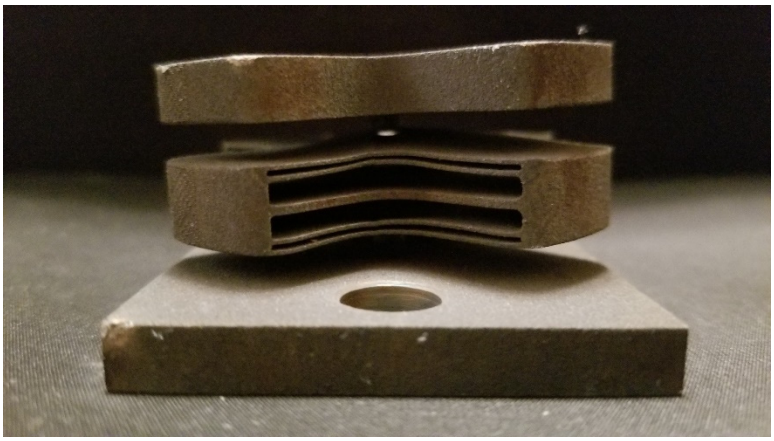

Figure 11. Heat Treat Damage

Finite Element Analysis

Finite Element Analysis (FEA) was conducted using Abaqus/Explicit 2017. A combination of solid and shell elements were used to create the finite element mesh. A part with the shell thickness rendered, is shown in Figure 12. The Abaqus S4R shell element, with enhanced hourglass control, was used to model the curved beams. The S4R element, is a quadrilateral shell with reduced integration. The Abaqus C3D8R element, with enhanced hourglass control, was use to mesh the remaining parts of the model, including the bumpers.

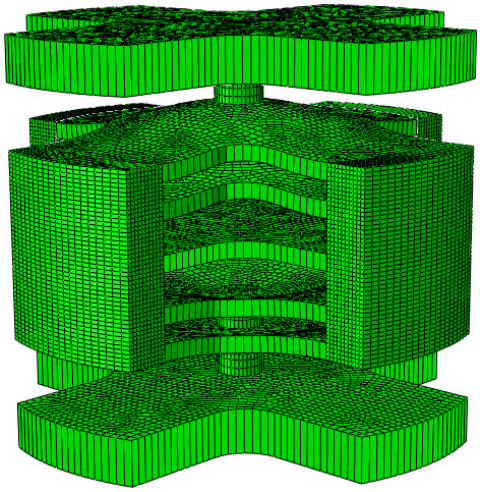

Figure 12. Shell / Solid Combination Mesh

Controlled displacement simulations were conducted to simulate the quasi-static tests and dynamic impact tests. For quasi-static simulations, a rigid body compressed the top of the specimen at a controlled rate, while the bottom of the specimen was minimally constrained. For the impulse simulations, the bottom nodes of the specimen were constrained using a prescribed node velocity.

Quasi-Static Testing

The first test to be conducted on the specimens was a quasi-static test. The test was conducted on a MTS Load Frame with a 100 kN load cell and fixed compression platens, at a rate of 2 mm/min. Figure 13 shows the unfiltered data from the test. There are no large spikes in force at maximum displacement because the MTS was programmed to begin unloading the specimen immediately before it fully compressed.

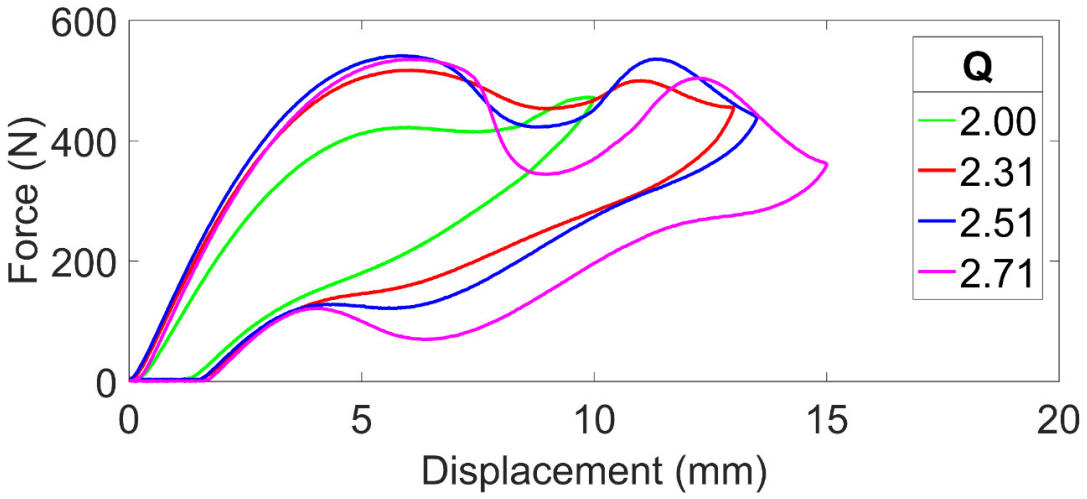

Figure 13. Nylon Quasi-static Test

Four different types of specimens were manufactured, with differing Q values. With a Q value of 2.00, the force threshold is low, shows little negative stiffness, and has a large flat region of zero stiffness. The energy absorbed, (area between the load and unload curve), is also low. As the Q value is increased to 2.31, the force threshold becomes much higher, and two humps become visible in the plot, one for each row "snapping" through. Much more energy is also absorbed. As the Q value is increased further, the humps become more pronounced, and the energy absorption is also increased. If specimens were built with a Q value greater than 2.71, they would likely be bistable. For a bistable specimen, as one of the beams snapped through, the force would become negative.

The force thresholds obtained experimentally are compared to those obtained from FEA and analytical approximations in Table 3. For the specimen with a Q value of 2.51, the FEA yielded a force threshold of 549.7 N, which is very close to the actual force threshold of 541.1 N. Using the two column analytical approximation outlined in Figure 5 yields a force threshold of 543.5 N, which is also very close to the actual force threshold. For the Q value of 2.71, the force threshold estimated using the analytical method is 663.2 N, vs 535.3 N actual, while the FEA predicted 538.0 N. The analytical method assumes rigid boundary conditions for the beams, which can over predict the force threshold, especially for high Q values.

Table 3 Nylon Quasi-Static Test Comparison

Bistability Parameter	**2.51**	**2.71**
Quasi-Static Test	541.1 N	535.3 N
Finite Element Analysis	549.7 N	538.0 N
Analytical	543.5 N	663.2 N

A simple quasi-static test was conducted on the metal specimens at a rate of 5mm/min. Figure 14 shows the results of the first test cycle for the three damaged specimens. Specimen #1 had the most damage and was tested first. The beginning of the test for specimen #1, shows a linear portion, which is caused by the compression platens correcting the slope of the top platform from a damage-induced slant to a horizontal position. The compression platens were held fixed to ensure that the top and bottom of the specimens were nominally parallel. The snap through of the first specimen was so loud that the technician stopped the test, as he thought the specimen had shattered. The test was then restarted, which explains the unload, load pattern for the first specimen. All four of the specimens exhibited a loud snap through sound for the first test. On all four specimens, the bottom beam was the first to snap through, represented by the first substantial decrease in force. After the first row snapped through, the force climbs again as the top beam is loaded. The top beam snaps through similarly to the bottom beam, but not as abrupt, and with less of a snapping sound. The second snap through is represented by the second substantial decrease in force. With both beams snapped through, the load is shunted to the bumpers causing the force to spike and the test to be terminated.

All four of the specimens exhibited bistable behavior under quasi-static conditions, which was expected because of the very high Q value of the design. The thickness of the center beam also helped maintain the rigidity of the beam boundary conditions, contributing to the bistable response.

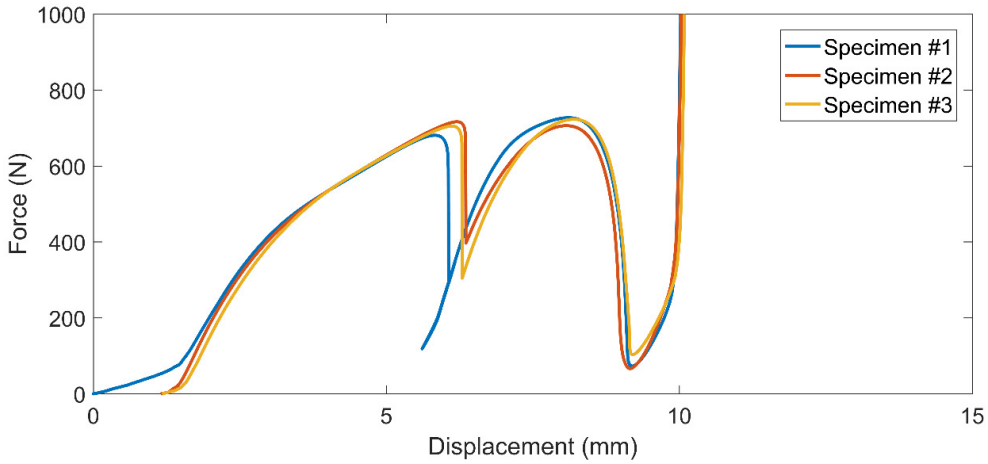

Figure 14. Metal Quasi-Static Test

All of the specimens were tested multiple times to investigate the repeatability of their force-displacement behavior. All three tests for specimen #2 are shown in Figure 15. The pronounced reduction in force threshold for the beams is due to plastic deformation, most likely where the beams attach to the bumpers. This area hardens however, leading to very repeatable results in the second and third tests.

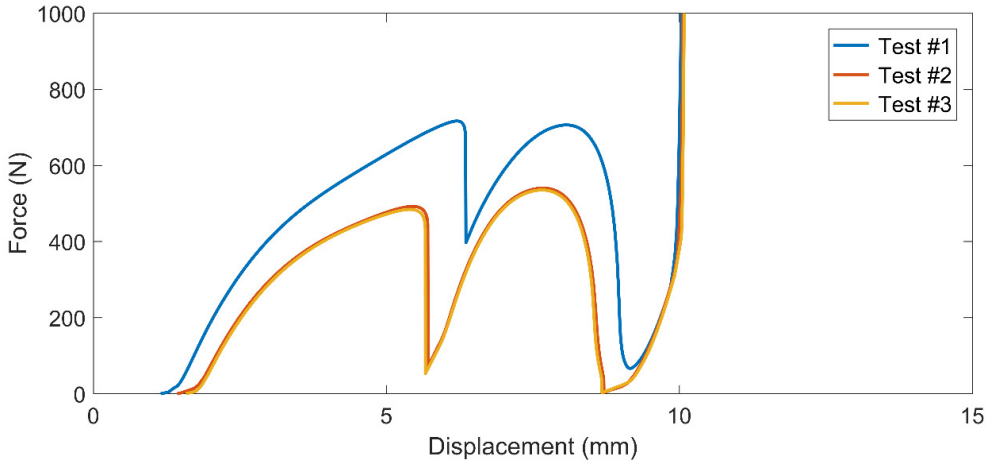

Figure 15. Specimen #2 Quasi-static Tests

The results of quasi-static testing of an undamaged Specimen #4 are compared with FEA in Figure 16. Due to an error by the manufacturer, specimen #4 was not included in first batch of parts sent to HIP, so it did not undergo the sagging deformation observed in the other specimens. It was heat treated to H1150 without HIP while oriented on its side, as in Figure 10. This prevented the damage seen in the other specimens. Due to its undamaged configuration, its initial force-displacement behavior is more linear than the damaged specimens. However, the force threshold remains similar, showing the robustness of the design.

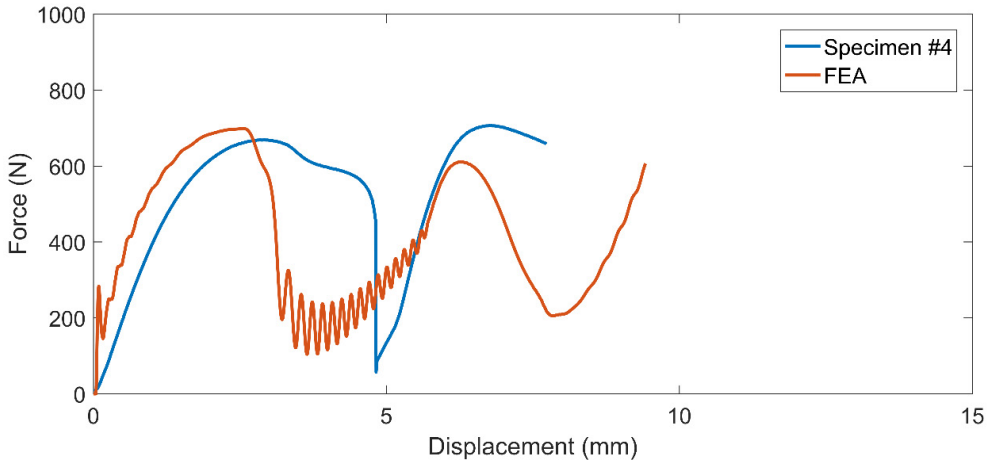

Figure 16. Quasi-static Testing of Undamaged Specimen #4 vs. FEA

The FEA in Figure 16 was conducted using material data from a DMLS build with the same HIP and heat treatment process as the specimens. For the metal design a plastic model was also used in conjunction with the elastic model, in order to provide accurate results when the load approaches the yield strain. The Young's Modulus of the material was 191.5 GPa, with a 0.2% yield stress of 839.5 MPa. This is very different from the manufacturer provided values in Table 2, and results in a yield strain of 0.00638, which is far lower than the yield strain for which the beams were designed. This is likely the reason for the large amounts of plastic deformation seen in Figure 15.

The FEA analysis closely represents the actual test, with a simulated force threshold of 698.4 N versus an experimental force threshold of 706.3 N. The exact load curve does not match, likely due to differences between the model and the actual specimen, and due to kinetic energy error of the explicit FEA analysis, which simulates the compression test at a rate much faster than the quasi-static rate for computational efficiency.

Drop Testing

Drop tests were conducted on the first three metal specimens, using two different machines of the same operating type. As shown in Figure 18, the machines have a large boxed steel frame, on which two cylindrical rails are bolted in the vertical position. A large carriage rides on these cylindrical rails, and can be raised to a maximum height of approximately 15 feet. The carriage is also bungee assisted, to allow for greater impact velocities. The specimen is typically bolted to the top of the carriage, and the load is transferred to the specimen when the carriage impacts a large metal reaction mass at the bottom of the rig. Felt, paper, and other materials are used to program the duration of the impulse. The technician fine tunes the impulse by adjusting the drop height, and programming material. Figure 17 shows a 15,000 g haversine impulse, with a 0.1 ms duration. The impulse is measured via an accelerometer mounted on top of the carriage, and an accelerometer mounted to the top of the specimen. The difference between the two accelerometer outputs shows the relative effectiveness of the specimen.

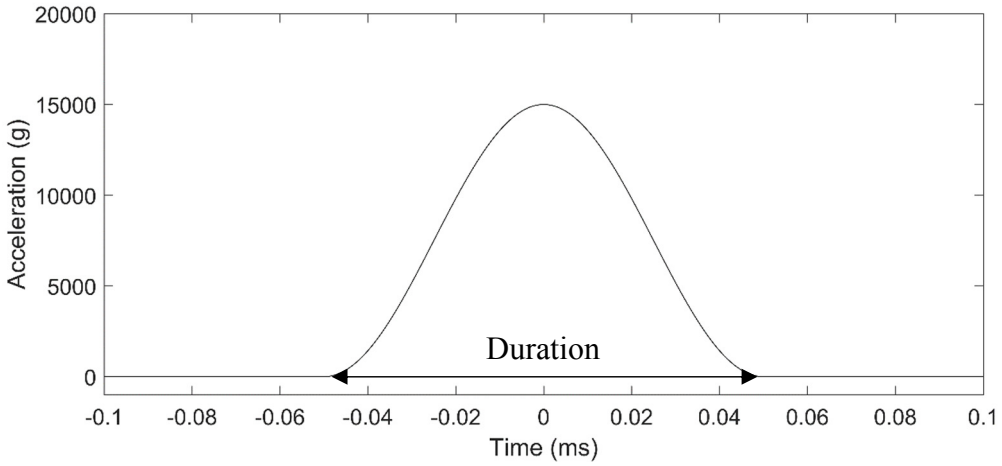

Figure 17. 15,000 g Haversine Impulse

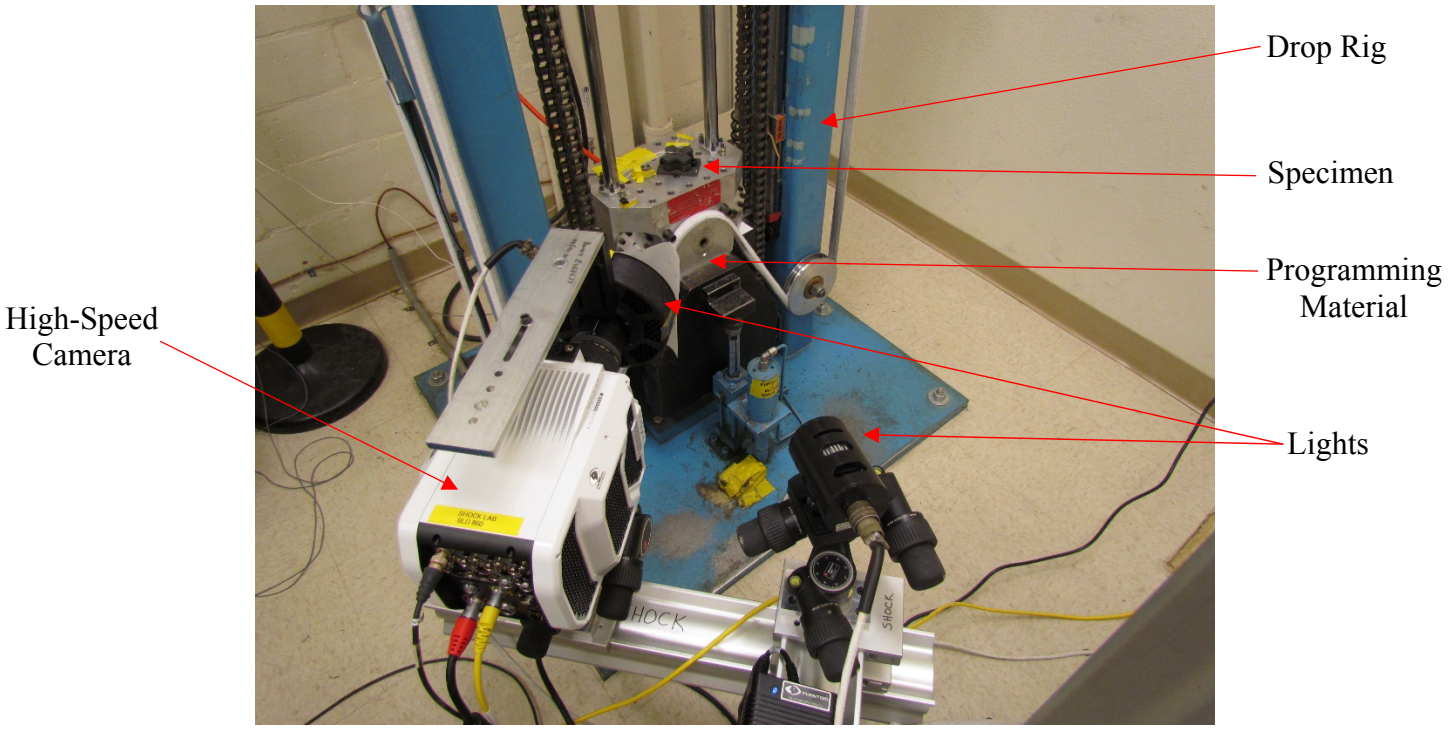

Figure 18. Drop Test Equipment

Figure 19 shows the result of a severe impulse with a duration of 0.088 ms. All of the data in Figure 19, was sampled at 2.5 MHz, and filtered using a 3rd order Butterworth filter, with a low pass cut off frequency of 10 kHz. The maximum acceleration measured from the top of the specimen is 758.3 g versus a peak carriage acceleration of 11,700 g. The design has the effect of reducing the peak acceleration but extending the duration of the impact event.

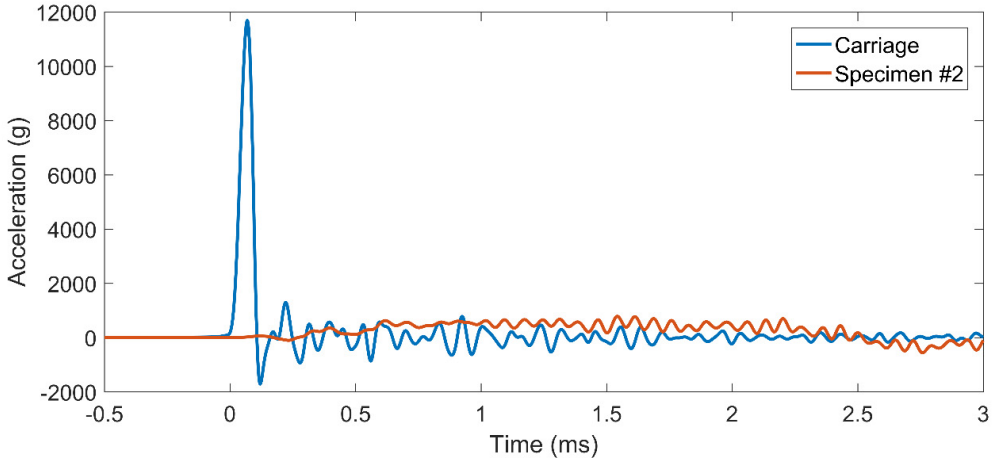

Figure 19. Specimen #2, 11,700 g impulse

Figure 20 shows the impulse response of specimen 3 for three tests with approximately the same input impulse. As shown, the specimen's impulse response is very repeatable.

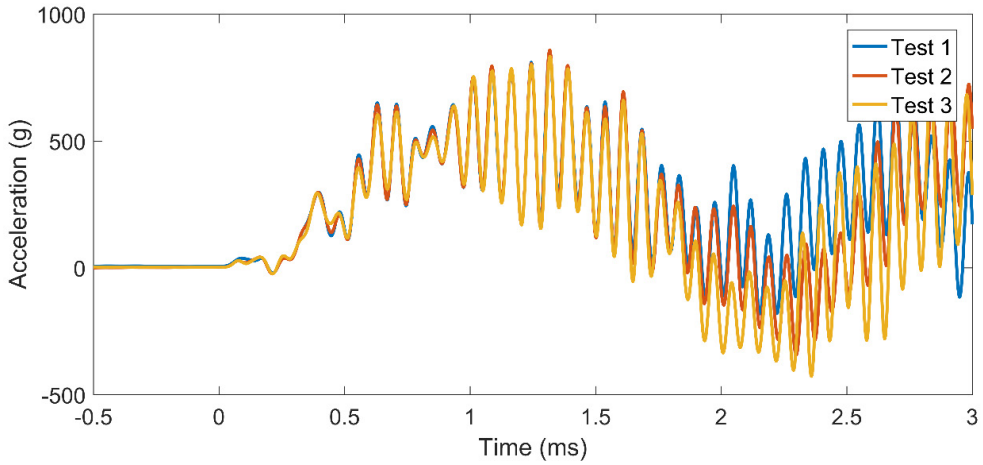

Figure 20. Specimen #3, 7900 g impulse

To simulate this impulse in Abaqus/Explicit, the acceleration is integrated to provide a constrained node velocity for the bottom nodes of the specimen. For the case of the 15,000 g, 0.1 ms impulse, the entire element is assigned a prescribed velocity of -7.355 m/s. As the simulation begins, the bottom nodes are decelerated using the constrained node velocity in Figure 21.

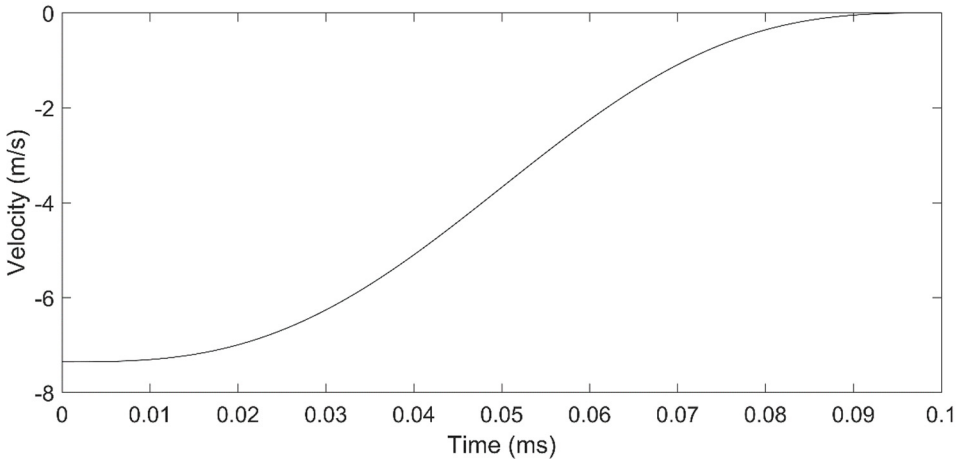

Figure 21. Constrained Node Velocity

Figure 22 compares the Abaqus/Explicit predictions versus the experimental performance of specimen 2. The peak acceleration agrees very closely between experiment and simulation: 784.8 g experimental versus 758.3 simulated. Differences can be attributed to several assumptions that are made in the finite element model. The first assumption is that the structure has not been stressed before the simulation. In reality, the specimen has already undergone quasi-static testing, which led to plastic deformation. This has the effect of making the specimen less resistant to severe impulses, which is observed in Figure 22 in the lower force threshold and the increase in time required to respond to the input impulse. Future work is being done to incorporate a deformed mesh and material state as an initial state for the impulse model. This will allow the designer to run a controlled displacement simulation first, and then input the

plastically deformed results into the impulse simulation. The second assumption is the use of the simplified input impulse shown in Figure 17. In reality the acceleration does not return to zero after the event. The carriage has some upward momentum after its impact with the reaction mass and before the brakes are engaged. In order to decrease the analysis time this behavior is not modeled, but could be included later if more accuracy is desired.

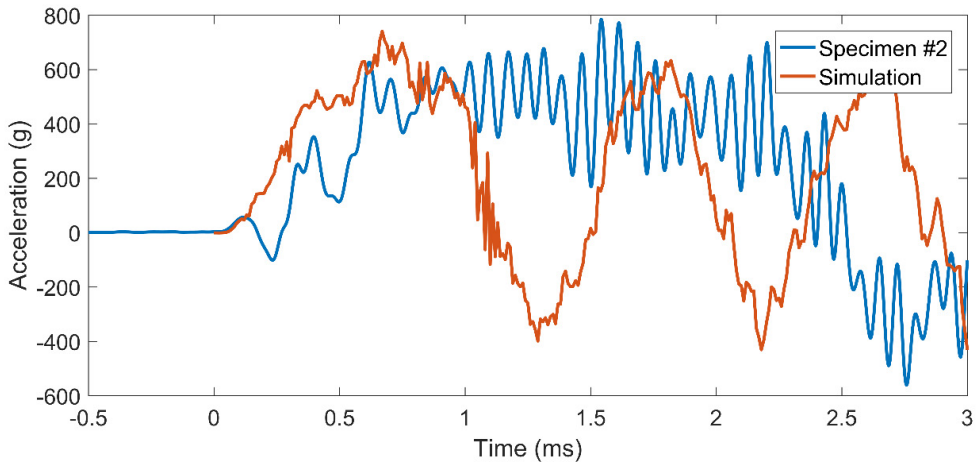

Figure 22. Specimen #2 vs. Abaqus Simulation

The first three metal specimens also exhibited damage from the heat treat. The simulation model did not account for this damage. The damage did not appear to have a significant effect on the dynamic response of the parts, but the damage did prevent testing at higher acceleration levels. Originally, the specimens were to be tested at a maximum level of 15,000 g, but on several 10,000 g tests, the base of the honeycomb descended at an angle, causing a large spike in acceleration due to the shunting of the load. This phenomenon is shown in Figure 23, and it is likely caused by the sagging and warping of the curved beams. Increasing the load would have resulted in more acceleration spikes, which are not ideal for impact mitigation. It is suspected that specimen #4, would not have descended at an angle, allowing it to be tested at higher g levels.

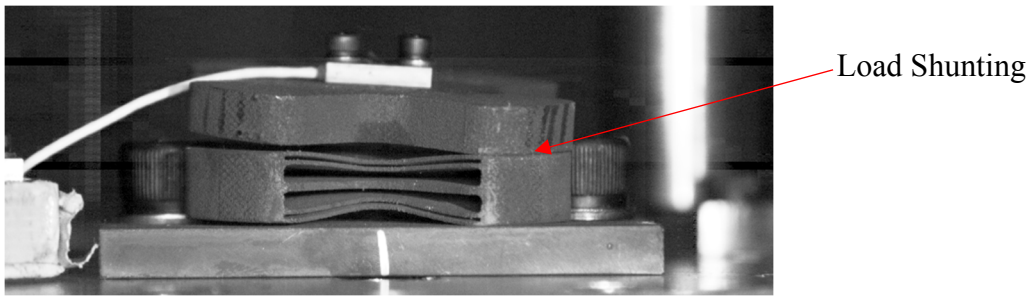

Figure 23. Load Shunting on 10,000 g Test

Conclusion

The conformal metal negative stiffness design shows much promise as an impact mitigation tool. The ability to tile the design, allows engineers to protect complex three dimensional surfaces against impacts from multiple directions. Since the design is made of stainless steel, it is resistant to heat, and can be used in unforgiving environments. Very severe impacts in the thousands of g's can be reduced by an order of magnitude, which allows system engineers more freedom in placing sensitive components.

Acknowledgments

This research was supported by an LDRD project from Sandia National Laboratories, entitled, "Additively Manufactured Shock Absorbing Engineered Materials." Testing would have been impossible without the support of Sandia National Laboratories in Albuquerque, New Mexico. We would like to thank Tommy Woodall, Nicholas Leathe, and Audrey Morris-Eckart, for their help in scheduling testing, and providing design requirements. We would also like to thank Matthew Spletzer, and all the technicians and engineers at the Shock Lab, who spent weeks drop testing specimens, and providing subject matter expert support.

References

[1] T. A. Schaedler, A. J. Jacobsen, A. Torrents, A. E. Sorensen, J. Lian, J. R. Greer, L. Valdevit and W. B. Carter, "Ultralight Metallic Microlattices," *Science,* vol. 334, no. 6058, pp. 962-965, 2011.

[2] X. Zheng, H. Lee, T. H. Weisgraber, M. Shusteff, J. DeOtte, E. B. Duoss, J. D. Kuntz, M. M. Biener, Q. Ge, J. A. Jackson, S. O. Kucheyev, N. X. Fang and C. M. Spadaccini, "Ultralight, ultrastiff mechanical metamaterials," *Science,* vol. 344, no. 6190, pp. 1373-1377, 2014.

[3] D. Restrepo, N. D. Mankame and P. D. Zavattieri, "Phase transforming cellular materials," *Extreme Mechanics Letters,* vol. 4, pp. 52-60, 2015.

[4] A. Rafsanjani, A. Akbarzadeh and D. Pasini, "Snapping Mechanical Metamaterials under Tension," *Advanced Materials,* vol. 27, no. 39, pp. 5931-5935, 2015.

[5] S. Shan, S. H. Kang, J. R. Raney, P. Wang, L. Fang, F. Candido, J. A. Lewis and K. Bertoldi, "Multistable Architected Materials for Trapping Elastic Strain Energy," *Advanced Materials,* vol. 27, no. 29, pp. 4296-4301, 2015.

[6] B. Haghpanah, L. Salari-Sharif, P. Pourrajab, J. Hopkins and L. Valdevit, "Multistable Shape-Reconfigurable Architected Materials," *Advanced Materials,* vol. 28, no. 36, pp. 7915-7920, 2016.

[7] D. M. Correa, T. Klatt, S. Cortes, M. Haberman, D. Kovar and C. Seepersad, "Negative stiffness honeycombs for recoverable shock isolation," *Rapid Prototyping Journal,* vol. 21, no. 2, pp. 193-200, 2015.

[8] D. M. Correa, C. C. Seepersad and M. R. Haberman, "Mechanical design of negative stiffness honeycomb materials," *Integrating Materials and Manufacturing Innovation,* vol. 4, no. 1, pp. 1-11, 2015.

[9] D. Correa, K. Bostwick, P. S. Wilson, M. Haberman and C. C. Seepersad, "Mechanical Impact Performance of Additively Manufactured Negative Stiffness Honeycombs," in *Solid Freeform Fabrication Symposium*, Austin, TX, 2015.

[10] J. Qiu, J. H. Lang and A. H. Slocum, "A curved-beam bistable mechanism," *Journal of Microelectromechanical Systems,* vol. 13, no. 2, pp. 137-146, 2004.